

Electronic versus Lattice Match for Metal-Semiconductor Epitaxial Growth: Pb on Ge(111)

S.-J. Tang,^{1,2,*} Chang-Yeh Lee,² Chien-Chung Huang,¹ Tay-Rong Chang,¹ Cheng-Maw Cheng,² Ku-Ding Tsuei,^{2,1}
H.-T. Jeng,^{3,1} V. Yeh,⁴ and Tai-Chang Chiang⁵

¹Department of Physics, National Tsing Hua University, Hsinchu 30013, Taiwan

²National Synchrotron Radiation Research Center, Hsinchu 30076, Taiwan

³Institute of Physics, Academia Sinica, Nankang, Taipei 11529, Taiwan

⁴Department of Physics, National Dong Hwa University, Hualien 97401, Taiwan

⁵Department of Physics, University of Illinois at Urbana-Champaign, 1110 West Green Street, Urbana, Illinois 61801-3080, USA

(Received 20 February 2011; published 2 August 2011)

Lattice match is important for epitaxial growth. We show that a competing mechanism, electronic match, can dominate at small film thicknesses for metal-semiconductor systems, where quantum confinement and symmetry requirements may favor a different growth pattern. For Pb(111) on Ge(111), an accidental lattice match leads to a $\sqrt{3} \times \sqrt{3}$ configuration involving a 30° in-plane rotation at large film thicknesses, but it gives way to an incommensurate (1×1) configuration at small film thickness. The transformation follows an approximately inverse-film-thickness dependence with superimposed bilayer oscillations.

DOI: 10.1103/PhysRevLett.107.066802

PACS numbers: 68.55.A-, 61.05.jh, 68.65.Fg, 73.20.-r

Metal-semiconductor interfaces are key elements in device architecture. A matched atomic structure, with a low-energy density, is conducive to smooth epitaxial growth. An important question is, what governs the growth pattern for lattice mismatched cases? For example, Pb films grown on Si(111)- (1×1) adopt the low-energy close-packed (111) surface orientation [1–3], and Ag films grown on Ge(111)- (1×1) behave similarly [4]. Each system has a large lattice mismatch, and the overlayer, under smooth film growth conditions, retains its own lattice constant and assumes an incommensurate (1×1) parallel-epitaxy configuration, $I(1 \times 1)$ for short [5]. Prior studies of these systems have shown ample evidence for quantum confinement, which gives rise to discrete quantum well states (QWS) and thickness-dependent electronic structure [6]. As a result, the surface energy and stability exhibit damped oscillations as a function of film thickness that are responsible for a number of novel effects including preferred (or magic) thicknesses, stability oscillations, nonstochastic roughness, and reentrant bilayer growth [7–15]. While these diverse phenomena are well understood, the simple $I(1 \times 1)$ configuration has remained a puzzle. Is it related to quantum confinement as well, and how?

This work focuses on Pb(111) growth on Ge(111), a case of special interest. The mismatch between the Pb and Ge lattice constants 4.92 and 5.65 Å is 13%. However, if the Pb film is rotated by 30° from the $I(1 \times 1)$ configuration, the Pb (2×2) unit cell and the substrate $\sqrt{3} \times \sqrt{3}$ unit cell become well matched (Fig. 1). This $\sqrt{3}$ configuration, for short, should be the preferred epitaxial orientation, and it is indeed the case at large film thicknesses. However, the general tendency toward the $I(1 \times 1)$ in other systems suggests otherwise, and this is indeed the preferred structure at small film thicknesses. The competition between the

two configurations $\sqrt{3}$ and $I(1 \times 1)$ follows approximately an inverse-film-thickness dependence with superimposed bilayer oscillations. We show that this behavior is a consequence of quantum confinement based on symmetry considerations.

Pb overlayers in our experiment were grown on a Ge(111) surface terminated by a monolayer (ML) of Pb to form a $\sqrt{3} \times \sqrt{3} - R30^\circ$ surface in the β phase [16]. The deposition and subsequent measurements were performed with the substrate maintained at -150°C . The Pb film thickness quoted below does not include the ML of the β phase. Discrete evolution of the quantum well peaks for increasing Pb coverage as observed by angle-resolved photoemission in the normal-emission direction [Fig. 2(a)] permits absolute determination of the film thickness. The films are atomically uniform at integer ML coverages. The photoemission measurements were performed by using 21.2 eV photons from a He lamp or synchrotron radiation from beam line 21B1-U9 at the National Synchrotron Radiation Research Center in Taiwan.

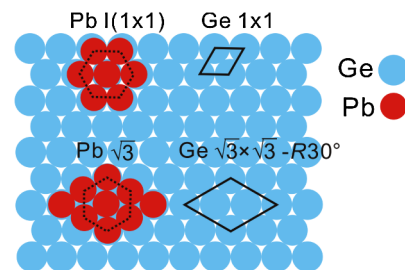


FIG. 1 (color online). Schematic diagrams for the Ge(111)- (1×1) substrate surface, a Ge(111)- (1×1) unit cell, a Ge(111)- $\sqrt{3} \times \sqrt{3} - R30^\circ$ unit cell, a Pb $I(1 \times 1)$ domain, and a Pb $\sqrt{3}$ domain.

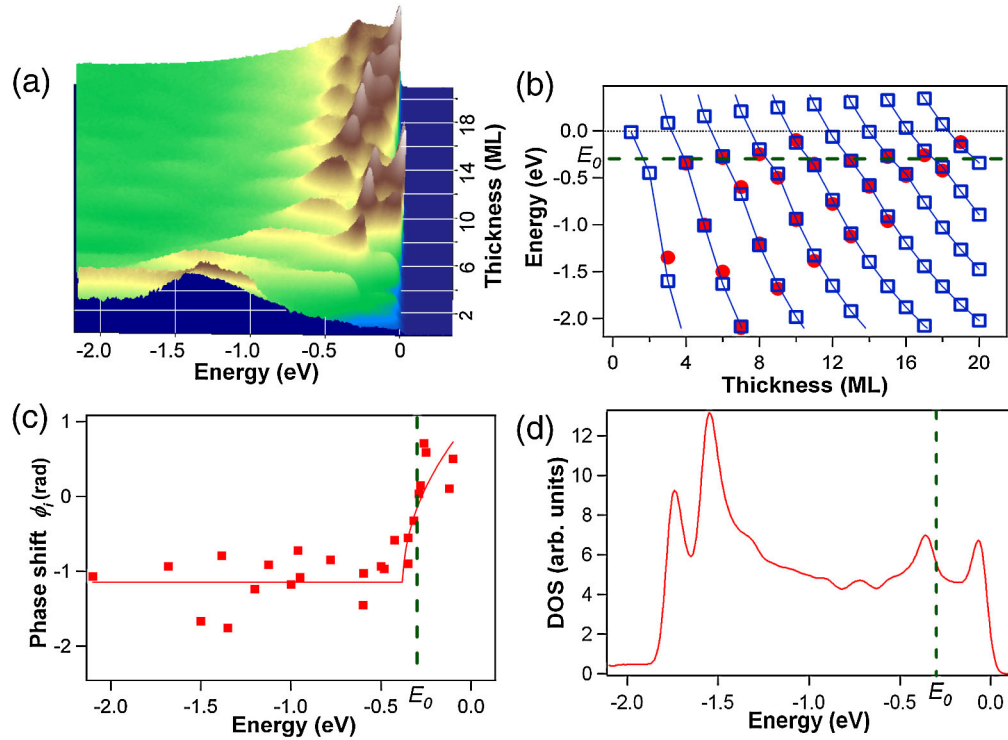


FIG. 2 (color online). (a) Angle-resolved photoemission intensity at normal emission as a function of energy and Pb overlayer thickness. (b) Energies of QWS at $\bar{\Gamma}$ from the experiment (red circles) and fitting (blue squares). E_0 indicates the Ge split-off band edge. (c) Interfacial phase shifts derived from fitting (solid curve) and the experiment (red squares). (d) One-dimensional density of states at $\bar{\Gamma}$ of the Ge substrate from first-principles calculations.

Angle-resolved photoemission mapping of Pb overlayers of thicknesses 2, 4, 6, 8, and 15 ML along the $\bar{\Gamma}\bar{K}$ direction yield spectral functions shown in Fig. 3(a). At 2 ML, the results closely resemble the k -resolved one-dimensional density of states of the Ge bulk band structure because of a strong hybridization of the Pb and Ge states and the large contribution from the Ge states within the photoemission probing depth [17,18]. The results are well explained by the model spectral function [17]:

$$A(k_{\parallel}, E) \propto \sum_{i=1}^3 |\langle \Psi_{\text{Pb}} | V_i | \Psi_{\text{Ge}} \rangle|^2 g_i(k_{\parallel}, E), \quad (1)$$

where the hybridization matrix element $\langle \Psi_{\text{Pb}} | V_i | \Psi_{\text{Ge}} \rangle$, with $i = 1, 2$, and 3 for the three Ge valence bands, is each taken to be a constant in the thin film limit, k_{\parallel} is the in-plane wave vector, and $g_i(k_{\parallel}, E)$ is the density of states of Ge. The model fits [right panel, Fig. 3(a)] are in good agreement with the data, where the dashed curves indicate the edges of the heavy-hole, light-hole, and split-off hole bands of Ge. These band dispersions were derived from first-principles calculations based on the full-potential projected augmented wave method as implemented in the VASP package [19,20]. Calculations based on the same method have also been performed for films for comparison with experiment.

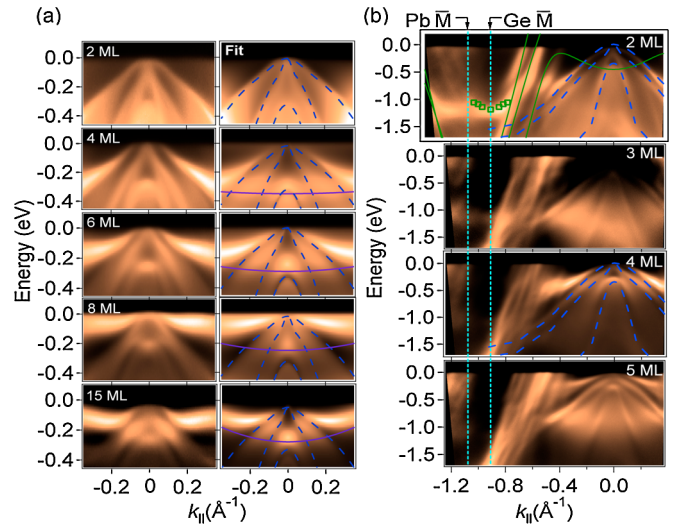


FIG. 3 (color online). (a) Left panel: Angle-resolved photoemission results along $\bar{\Gamma}\bar{K}$ for Pb film thicknesses of 2, 4, 6, 8, and 15 ML. Right panel: Model fits to the data. The dashed curves indicate the Ge band edges. The solid curves indicate QWS subbands from the fits. (b) Angle-resolved photoemission results along $\bar{\Gamma}\bar{M}$. The Ge band edges are shown by dashed curves. The solid green curves for 2 ML are calculated QWS subbands for a freestanding film. The green squares represent the calculated dispersion of a QWS subband of the second kind. The \bar{M} points of Ge and Pb are indicated.

The data at higher coverages (4–15 ML) in Fig. 3(a) are quite different; an Anderson model involving a hybridization interaction of the discrete Pb QWS subbands and the Ge states [4] is used to construct a model spectral function:

$$A(E) = -\frac{1}{\pi}\text{Im}(G) = -\frac{1}{\pi}\text{Im}\left(\frac{1}{E - E_q + i\delta_q - \sum_{i=1}^3 \pi A_i |V_i|^2 (E - E_0^i + i\delta_s^i)^{-1/2}}\right), \quad (2)$$

where the dependence on k_{\parallel} is not explicitly shown, E_q is the energy of the quantum well state without coupling, δ_q and δ_s^i are the lifetime broadenings of the QWS and the substrate states, respectively, and E_0^i is the Ge band edge. Results of the fitting, shown on the right-hand side of Fig. 3(a), match the data well. The solid purple curve shows $E_q(k_{\parallel})$, the dispersion of the “bare” QWS subband.

The corresponding data along $\bar{\Gamma}\bar{M}$ for 2–5 ML are shown in Fig. 3(b). Near $\bar{\Gamma}$, the spectral function at low coverages is dominated by the one-dimensional density of states of the Ge substrate. Indicated in the figure are the Ge bulk band edges (dashed curves) for reference. For k_{\parallel} between about -0.4 and -0.6 \AA^{-1} , a bundle of steeply downward dispersing QWS subbands in the Pb films is observed. They resemble the calculated dispersion relations for freestanding films (green curves for the 2 ML case). The two vertical dashed lines indicate the \bar{M} points of the Pb and Ge surfaces. Unique among the set, the 2 ML case shows a parabolic band, centered about the Ge \bar{M} point, and its mirror image about the Pb \bar{M} point. This is a QWS subband of the second kind, for which the confinement is caused by umklapp reflections at the Ge substrate surface [21]. A parallel-epitaxy $I(1 \times 1)$ configuration is crucial for the formation of this state. The green squares indicate the calculated dispersion relation.

From the fitting [Fig. 3(a)], the bare QWS energies at the zone center between 0 and -0.4 eV are extracted. Interference from the Ge band edges becomes minimal below -0.4 eV, and the quantum well peak positions are read off directly from the data [Fig. 2(a)]. These experimental values, shown as red circles in Fig. 2(b), are compared to a fit (blue squares) based on the Bohr-Sommerfeld quantization condition [6]

$$2k_{\perp}(N+1)t + \phi_i + \phi_s = 2n\pi, \quad (3)$$

where k_{\perp} is the perpendicular wave vector, $\phi_{i,s}$ are the phase shifts at the interface and surface, respectively, t is the Pb ML thickness, $N+1$ is the number of Pb MLs (+1 to include the ML of the β phase), and n is a quantum number. The surface phase shift ϕ_s is taken from a calculation [11]. A fit using a known analytic form of ϕ_i [22] yields the curve in Fig. 2(c); for comparison, the red squares indicate the values extracted from the Bohr-Sommerfeld condition. The results show a sharp rise at about -0.4 eV, which is very close to the Ge split-off band edge at about $E_0 = -0.3$ eV. This rise corresponds to a van Hove singularity and is a consequence of the analyticity of the scattering function across the band edge [22].

Low-energy electron diffraction measurements reveal the film growth orientation [Fig. 4(a)]. Patterns from the bare Ge(111)- $c(2 \times 8)$ and the Pb/Ge(111)- $\sqrt{3} \times \sqrt{3} - R30^\circ$ β phase establish the reference orientations and scale factors. Upon Pb coverage at 2 ML, the $\sqrt{3} \times \sqrt{3} - R30^\circ$ pattern is suppressed. An attenuated Ge(111)- (1×1) substrate pattern remains and is accompanied by six short arcs with the same orientation but farther out. The radius of the arcs indicates an $I(1 \times 1)$ Pb overlayer. The arc lengths indicate a mosaic structure; so, the tendency for orientational order has a relatively broad energy minimum. At higher coverages, each arc splits into a pair of spots at about $\pm 5^\circ$; thus the domains become locked into two symmetry-equivalent slightly twisted (111) orientations that are determined by the best near-lattice match around the $I(1 \times 1)$ configuration (coincidence lattice configuration) [3,23,24]. For simplicity, we continue to refer to these twisted domains as $I(1 \times 1)$ domains. Also evident in the data is the emergence of $\sqrt{3}$ domains at 3 ML which eventually dominates at higher Pb coverages. The

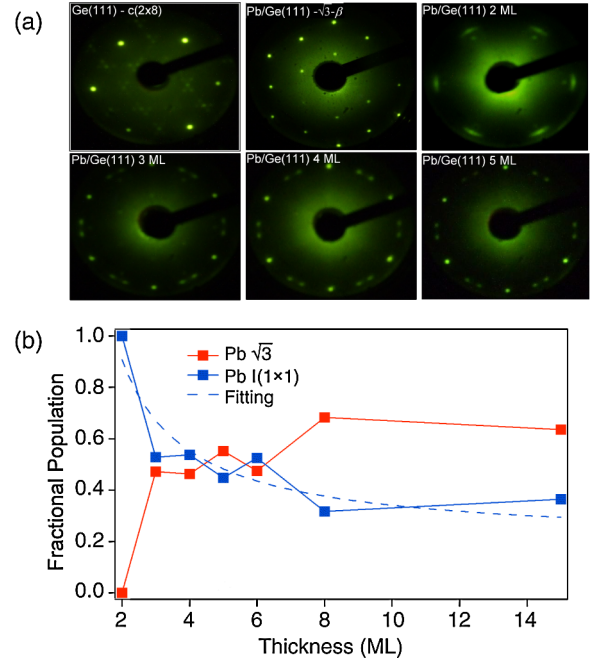


FIG. 4 (color online). (a) Low-energy electron diffraction patterns, taken with the beam energy at 40 eV, from Ge(111)- $c(2 \times 8)$, Pb/Ge(111)- $\sqrt{3} \times \sqrt{3} - R30^\circ$ β phase, and 2, 3, 4, and 5 ML of Pb overlayers. (b) Fractional populations for the $I(1 \times 1)$ and $\sqrt{3}$ configurations as a function of Pb overlayer thickness. The dashed curve is a fit assuming a $1/N$ dependence.

fractional populations of $I(1 \times 1)$ and $\sqrt{3}$ domains are deduced from the low-energy electron diffraction intensities [Fig. 4(b)]. The dashed curve is a fit to the $I(1 \times 1)$ population assuming a C/N dependence [25,26] with $C = 1.41$.

Two competing factors are at play: One is the interfacial energy, which is independent of the film thickness and favors the $\sqrt{3}$ lattice-matched configuration, and the other is the electronic energy associated with quantum confinement, which diminishes as $1/N$ and also depends on the degree of electronic hybridization across the Pb-Ge interface. A strong hybridization as a result of electronic match minimizes the effects of confinement, leading to a lower system energy. We argue below that the $I(1 \times 1)$ configuration presents a much better electronic match than the $\sqrt{3}$ configuration based on general symmetry considerations. Thus, the $I(1 \times 1)$ configuration is preferred at small thicknesses for Pb/Ge(111), and it is the sole configuration adopted by Ag/Ge(111)-(1 \times 1) and Pb/Si(111)-(1 \times 1), where a rotated, accidentally matched configuration does not exist.

The symmetry property of interest concerns the $\{1\bar{1}0\}$ mirror planes separated at 60° intervals in both Ge and Pb. Electronic states with wave vectors on these symmetry planes are of definite parity. States in Ge and Pb would be well coupled if they are of the same parity. This is the case for the $I(1 \times 1)$ configuration where the Pb and Ge share the same mirror operations, and the coupling potential V_i in Eqs. (1) and (2) is an even function. States off but near these mirror planes remain well coupled as the deviation in parity is a second-order effect. For this reason, the system would be tolerant to a small angular rotation of the film relative to the substrate. This explains the mosaic spread of the domains at 2 ML and the approximately $\pm 5^\circ$ twisted coincidence lattice configuration at higher coverages. The electronic mismatch becomes the greatest when the relative rotation of the Pb and Ge lattices reaches 30° . The parity mixing at the interface causes decoupling of the Pb and Ge states, leading to an enhanced confinement and an overall increase in system energy. The $\sqrt{3}$ configuration thus has a higher energy, but the energy difference decays as $1/N$. When N becomes large, the interfacial term takes over, and the system should transform from $I(1 \times 1)$ to $\sqrt{3}$.

Each population curve in Fig. 4(b) exhibits a superimposed bilayer oscillation pattern for $N = 2-6$, which is reminiscent of the one-dimensional shell effects associated with quantum confinement with a period of oscillation equal to one-half of the Fermi wavelength, or 2.2 ML [26]. Even N values of 2, 4, and 6 are more favorable for the $I(1 \times 1)$ configuration than the intervening odd N values [Fig. 4(b)]. A QWS subband happens to lie close to E_0 for $N = 2, 4, \text{ and } 6$ [Fig. 2(b)], where the one-dimensional Ge density of states shows a peak [Fig. 2(d)]. This coincidence implies a stronger hybridization and a

lower confinement energy for the $I(1 \times 1)$ configuration, thus enhancing the $I(1 \times 1)$ population. This effect, not present for $N = 3$ and 5, leads to the bilayer oscillations. The system becomes fully $I(1 \times 1)$ at 2 ML, and this is the only case exhibiting a quantum well subband of the second kind [Fig. 2(b)]. At higher coverages, the $I(1 \times 1)$ domains become fragmented, making the second-kind states unobservable.

Our electronic-match model thus explains a long-standing puzzle of why mismatched metal-semiconductor interfaces such as Ag/Ge(111) and Pb/Si(111) adopt the $I(1 \times 1)$ growth orientation. Pb/Ge(111), with an accidental lattice match for the $\sqrt{3}$ configuration, is well suited for testing the competing effects between electronic match and lattice match. The general understanding established in the present study is important for devising strategies for smooth film growth with prescribed configurations—a key issue relevant to thin film electronics.

This research is supported by the National Science Council of Taiwan (Grants No. NSC 98-2112-M-007-017-MY3 and No. NSC 95-2112-M-007-062-MY3 for S.-J. T.) and the U.S. Department of Energy, Basic Energy Sciences (Grant No. DE-FG02-07ER46383 for T.-C. C.). Much of the work was performed at the National Synchrotron Radiation Research Center of Taiwan. We thank C. M. Wei for helpful discussions.

*sjtang@phys.nthu.edu.tw

- [1] M. Upton, C. M. Wei, M. Y. Chou, T. Miller, and T.-C. Chiang, *Phys. Rev. Lett.* **93**, 026802 (2004).
- [2] W. B. Jian, W. B. Su, C. S. Chang, and T. T. Tsong, *Phys. Rev. Lett.* **90**, 196603 (2003). The two island domains reported therein correspond to different stacking sequences (or twining). Twining is minimized under smooth film growth conditions as reported in [1].
- [3] M. Hupalo, V. Yeh, T. L. Chan, C. Z. Wang, K. M. Ho, and M. C. Tringides, *Phys. Rev. B* **71**, 193408 (2005).
- [4] S.-J. Tang, L. Basile, T. Miller, and T.-C. Chiang, *Phys. Rev. Lett.* **93**, 216804 (2004).
- [5] A number of metals grow similarly on the Si(111)-(7 \times 7) surface. The strong corrugation of the (7 \times 7) reconstruction could pin the overlayer orientation. These cases are not considered here.
- [6] T.-C. Chiang, *Surf. Sci. Rep.* **39**, 181 (2000).
- [7] D.-A. Luh, T. Miller, J. J. Paggel, and T.-C. Chiang, *Phys. Rev. Lett.* **88**, 256802 (2002).
- [8] L. Aballe, A. Barinov, A. Locatelli, S. Heun, and M. Kiskinova, *Phys. Rev. Lett.* **93**, 196103 (2004).
- [9] A. R. Smith, K.-J. Chao, Q. Niu, and C.-K. Shih, *Science* **273**, 226 (1996).
- [10] Zhenyu Zhang, Q. Niu, and C.-K. Shih, *Phys. Rev. Lett.* **80**, 5381 (1998).
- [11] C. M. Wei and M. Y. Chou, *Phys. Rev. B* **66**, 233408 (2002).
- [12] Y. Jia, B. Wu, H. H. Weitering, and Zhenyu Zhang, *Phys. Rev. B* **74**, 035433 (2006).

- [13] M. M. Özer, Y. Jia, B. Wu, Zhenyu Zhang, and H. H. Weitering, *Phys. Rev. B* **72**, 113409 (2005).
- [14] P. Czochke, H. Hong, L. Basile, and T.-C. Chiang, *Phys. Rev. Lett.* **93**, 036103 (2004).
- [15] M. Hupalo, V. Yeh, L. Berbil-Bautista, S. Kremmer, E. Abram, and M. C. Tringides, *Phys. Rev. B* **64**, 155307 (2001).
- [16] H. Morikawa, I. Matsuda, and S. Hasegawa, *Phys. Rev. B* **77**, 193310 (2008).
- [17] S.-J. Tang, T. Miller, and T.-C. Chiang, *Phys. Rev. Lett.* **96**, 036802 (2006).
- [18] S.-J. Tang, T.-R. Chang, C.-C. Huang, C.-Y. Lee, C.-M. Cheng, K.-D. Tsuei, H.-T. Jeng, and C.-Y. Mou, *Phys. Rev. B* **81**, 245406 (2010).
- [19] G. Kresse and J. Hafner, *Phys. Rev. B* **48**, 13 115 (1993).
- [20] G. Kresse and J. Furthmüller, *Phys. Rev. B* **54**, 11 169 (1996).
- [21] S.-J. Tang, Y. R. Lee, S.-L. Chang, T. Miller, and T.-C. Chiang, *Phys. Rev. Lett.* **96**, 216803 (2006).
- [22] D. A. Ricci, Y. Liu, T. Miller, and T.-C. Chiang, *Phys. Rev. B* **79**, 195433 (2009).
- [23] H. Li and B. P. Tonner, *Surf. Sci.* **193**, 10 (1988).
- [24] W. E. McMahon, E. S. Hirschorn, and T.-C. Chiang, *Surf. Sci. Lett.* **279**, L231 (1992).
- [25] Y. Liu, N. J. Speer, S.-J. Tang, T. Miller, and T.-C. Chiang, *Phys. Rev. B* **78**, 035443 (2008).
- [26] T. Miller, M. Y. Chou, and T.-C. Chiang, *Phys. Rev. Lett.* **102**, 236803 (2009).